ACCELERATED PUBLICATION

An Exclusion Mechanism in Ion Exchange Chromatography

C. Harinarayan,[1] J. Mueller,[1] A. Ljunglöf,[2] R. Fahrner,[1] J. Van Alstine,[2] R. van Reis[1]

[1]Genentech Inc., South San Francisco, California; telephone: 650-225-1522; fax: 650-225-4049; e-mail: rvr@gene.com
[2]GE Healthcare, Bio-Sciences AB, SE-751 84 Uppsala, Sweden

Received 13 March 2006; accepted 13 June 2006

Published online 8 August 2006 in Wiley InterScience (www.interscience.wiley.com). DOI: 10.1002/bit.21080

Abstract: Protein dynamic binding capacities on ion exchange resins are typically expected to decrease with increasing conductivity and decreasing protein charge. There are, however, conditions where capacity increases with increasing conductivity and decreasing protein charge. Capacity measurements on two different commercial ion exchange resins with three different monoclonal antibodies at various pH and conductivities exhibited two domains. In the first domain, the capacity unexpectedly increased with increasing conductivity and decreasing protein charge. The second domain exhibited traditional behavior. A mechanism to explain the first domain is postulated; proteins initially bind to the outer pore regions and electrostatically hinder subsequent protein transport. Such a mechanism is supported by protein capacity and confocal microscopy studies whose results suggest how knowledge of the two types of IEX behavior can be leveraged in optimizing resins and processes. © 2006 Wiley Periodicals, Inc.

Keywords: ion exchange chromatography; binding capacity; exclusion; antibodies; mAb; proteins; confocal microscopy

INTRODUCTION

Ion exchange chromatography (IEX) is used extensively in the biotechnology industry to purify monoclonal antibodies as well as other proteins (Gagnon, 1996; Janson and Ryden, 1998). IEX is based on differential adsorption of charged substances at oppositely charged surfaces of porous chromatographic media. The strength of such interactions and the adsorption capacity of the IEX media are assumed to vary inversely with conductivity (Janson and Ryden, 1998). Several models describe the complex adsorption mechanisms in IEX (Brooks and Cramer, 1992; Chang and Lenhoff, 1998; Gallant, 2004; Hunter and Carta, 2000; Lewus and Carta, 2001; Liapis et al., 2001; Nash and Chase, 1998; Zhang et al., 2004a). Confocal microscopy has recently been used to further elucidate the complex nature of IEX adsorption and transport mechanisms (Dziennik et al., 2003; Hubbuch et al., 2002, 2003; Kasche et al., 2003; Laca et al., 1999; Linden et al., 1999, 2002; Ljunglöf and Hjorth, 1996; Ljunglöf and Thömmes, 1998).

In a simplistic sense the dynamic binding (Q_B) of a protein to an ion exchange resin is expected to decrease with protein charge (opposite to that of the resin) and increasing ionic strength. Q_B typically decreases with increasing conductivity or as pH approaches protein isoelectric point (pI). This behavior has been well characterized. However, the authors previously observed capacity effects that do not conform to this well characterized behavior and proposed a mechanism that accounts for these effects (Harinarayan et al., 2002).

More recently other investigators have observed such departures from expected IEX behavior. For example, Hubbuch et al. (2003) studied adsorption of BSA to SP Sepharose XL at pH 4.5 and 5 in which confocal microscopy revealed that protein adsorption was restricted to the outer surfaces of the bead.

Important insights into mass transfer have been gained from both fundamental studies and practical applications in chromatography and ultrafiltration. Several studies relevant to this work are described below.

Smith and Deen (1980) presented a theoretical analysis of transport of spherically charged colloids in cylindrical charged pores. This model assumes the presence of an electrical double layer surrounding a charged solute or pore. When a charged solute partitions into a neutral pore, the ensuing compression of this electrical double layer creates a condition that is energetically unfavorable to the transport of the solute through the pore.

A compression of the double layer associated with a charged pore in the presence of a neutral solute will yield a similar effect. This exclusion effect is magnified when both

Correspondence to: R. van Reis

Abbreviations used: BSA, bovine serum albumin; IEX, ion exchange; MES, 2-(4-morpholino)-ethane sulfonic acid; QB10%, dynamic binding capacity at 10% breakthrough; SP, sulfopropyl.

pore and solute are charged. The Smith and Deen model has been successfully applied to membrane separations (Pujar and Zydney, 1994).

Exclusion effects have been observed in size exclusion chromatography (SEC) (resin with slight charge) under specific buffer conditions. For example, it was demonstrated that pH and ionic strength of load buffers significantly affected the retention of various proteins (Potschka, 1988). The retention volume of myoglobin (pI = 7.3) in a TSK 5000PW (Toyo-Soda/LKB) column decreased with decreasing conductivity at pH 8 while the retention volume increased with decreasing conductivity at pH 6.6 (Potschka, 1988).

In conventional ultrafiltration, a neutral membrane retains neutral solutes by a size exclusion mechanism. The sieving behavior of charged solutes differs from that of neutral solutes in neutral membranes. Charged solutes have an electrical double layer due to electrostatic interactions with ions in solution. When a solute enters a pore, this electrical double layer is compressed if the size of the pore and solute are of the same order of magnitude. This is not favored energetically leading to a decrease in the sieving of the charged solute. Similar effects occur when applying a neutral solute to a charged membrane (Saksena and Zydney, 1994). A compression of the electrical double layer associated with the pore wall occurs due to the presence of the neutral solute. This effect is further magnified with like charged pores and solutes. Membranes with charged ligands exhibit lower sieving of proteins (of similar charge) due to charge repulsion (van Reis et al., 1999).

Exclusion effects seen in SEC and membranes have been correlated (Pujar and Zydney, 1998). Pujar and Zydney (1998) demonstrated the similarity of the electrostatic exclusion occurring in both by determining retention times in SEC and sieving coefficients in ultrafiltration membranes for BSA and dextrans.

The authors previously postulated an exclusion mechanism in IEX that reflects such adsorption reducing effective pore diameter and reversing pore net surface charge. The end result is that other protein molecules may be effectively excluded from transport into the resin, greatly limiting dynamic binding capacities (Harinarayan et al., 2002).

This exclusion mechanism requires that proteins initially entering a IEX media pore bind near the entrance and should therefore function to a greater extent in buffer solutions affording reduced conductivity and increased protein net charge (van Reis, 2005).

The present work involved a study of the exclusion mechanism in conventional cation exchange chromatography. Protein dynamic binding capacity studies were performed with monoclonal antibodies at varying pH and conductivity. These studies provided indirect evidence that protein exclusion effects in IEX are influenced by the strengths of both protein–protein and protein–media charge-based interactions. Confocal microscopy provided more direct, micron level visualization of chromatographic adsorption, transport, and exclusion effects.

Table I. Molecular weights and pI (capillary zone electrophoresis) of proteins studied.

Protein	Molecular Weight (kDa)	pI
Mab 1	160	9.2
Mab 2	160	7.4
Mab 3	160	7.5

MATERIALS AND METHODS

Proteins, Chemicals, and Resins

Cation exchange resins, SP Sepharose™ XL (198 μmol H^+/mL), and SP Sepharose Fast Flow (198 μmol H^+/mL) were obtained from GE Healthcare (Uppsala, Sweden). Dextrans were obtained from TdB Consultancy Inc. (Uppsala, Sweden). Cy3 and Cy5 reactive dyes were also obtained from GE Healthcare and Alexa 488 from Molecular Probes (Leiden, The Netherlands). Protein labeling was performed according to the standard procedure recommended by the manufacturers. Three full-length monoclonal antibodies from Genentech Inc. (South San Francisco, CA) were utilized. The molecular weights and pIs of the proteins are shown in Table I. Net charge versus pH for the proteins based on the amino acid sequence is given in Figure 1.

For pH 4 and 5 equilibration, load and wash buffers, 15mM Sodium acetate (Fisher Scientific, Hampton, NH) was used. The buffers were pH adjusted with glacial acetic acid (Mallinckrodt, Phillipsburg, NJ). For pH 6 buffers, 14 mM MES (Angus Buffers and Biochemicals, Buffalo Grove, IL) and 10 mM Sodium MES (Angus Buffers and Biochemicals) was used. The buffers were pH adjusted with 50% Sodium hydroxide (J.T Baker, Phillipsburg, NJ). Proteins (8 mg/mL) were diafiltered into the three different buffers. A stock solution of 5 M NaCl was added to obtain a range of conductivities from 1 to 50 mS/cm. A gradient elution was performed with equilibration buffer and buffer made up with 20 mM MES, 4.5 mM Sodium MES, 1.5 M NaCl, pH 5.5.

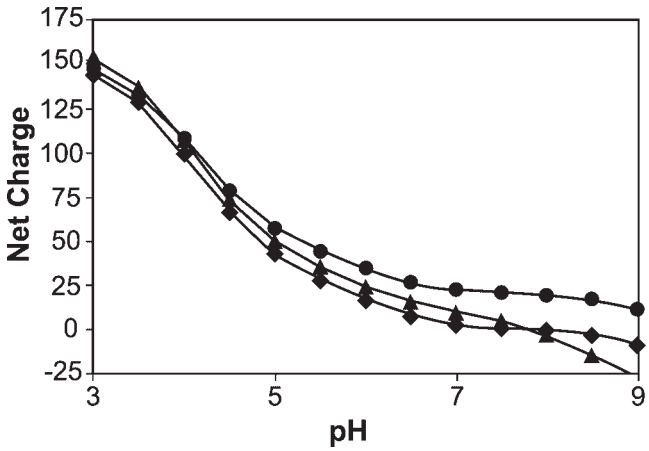

Figure 1. Net charge based on amino acid sequence as a function of pH for Mab1 (●), Mab2 (▲) and Mab3 (◆).

DOI 10.1002/bit

Table II. Peak molecular masses and viscosity radii of dextrans.

Dextran	Peak molecular mass* (kDa)	Viscosity radius** (nm)
1	1.06	0.87
10	10.4	2.71
40	37.8	5.16
110	99.5	8.35
500	450	17.71
800	710	22.23
2,000	2,050	37.69

*Supplied by manufacturer.
**$R_\eta = 0.271 \times M_p^{0.498}$ where R_η = Viscosity radius and M_p = Peak molecular mass (Hagel, 1988).

Dextran solutions were prepared at a concentration of 1 mg/mL, by dissolving each dextran into the appropriate buffer (pH 4 or 6, 1, 5 or 50 mS/cm). Glucose (1 mg/mL) was added to each dextran solution. 0.01% Sodium azide was added to each solution to prevent bacterial growth. Peak molecular masses and viscosity radii estimates for each dextran are given in Table II.

Columns with packed bed volumes of 3.4 mL, bed diameters of 0.66 cm, and bed heights of 10 cm (Biochem valve/Omnifit™, Boonton, NJ) were used in protein capacity studies. Columns with packed bed volumes of 60 mL, bed diameters of 1.6 cm, and bed heights of 30 cm (XK16/30, GE Healthcare, Uppsala, Sweden) were used in the resin characterization study.

Instrumentation

Chromatography experiments were performed on an ÄKTAexplorer™ 100 (GE Healthcare). A refractive index detector (RI 72, Shodex, Japan) was connected in line to the ÄKTA™ system for detection of dextrans and glucose. Confocal microscopy measurements were made with a Leica TCS SP confocal scanning laser microscope equipped with He/Ne and an argon laser, and with TCS NT software for image evaluation.

Protein Dynamic Binding Capacity

Dynamic binding capacities for Mab1, Mab2, and Mab3 were obtained at pH 4, 5, and 6 with conductivities of 1, 5, 10, 15, and 25 mS/cm on SP Sepharose XL and SP Sepharose FF. Additional conductivities (0.6, 2.5, 7.5, and 20 mS/cm) were tested in some cases to better define the capacity trends. The resins were equilibrated using three column volumes (CV) of the load buffer. The protein was loaded onto the resin to 10% breakthrough capacity ($Q_{B10\%}$) based on the protein load absorbance (A_{280}). Unbound proteins were washed away using 5 CV of the same buffer. Bound protein was eluted by a 6 CV gradient elution (0–100% elution buffer) using the equilibration buffer and elution buffer (20 mM MES, 4.5 mM Sodium MES, 1.5 M NaCl, pH 5.5), followed by 6 CV with elution buffer. Dynamic binding capacities were obtained according to Equation1.

$$Q_{B10\%} = \frac{(V_p - V_h)C_p}{V_b} \quad (1)$$

where V_p = volume of protein loaded at 10% breakthrough, V_h = hold up volume of system, C_p = concentration of protein loaded, and V_b = packed bed volume of resin.

Three experiments were performed for each condition. For additional conductivities (0.6, 2.5, 7.5, and 20 mS/cm) tested, two experiments were performed. Averages of triplicate or duplicate capacities are reported. The maximum standard deviation for replicate capacity values was 5 mg/mL. The yield was computed from the volumes and concentrations of the load and elution pools. All chromatography experiments were performed at ambient room temperature at a flow rate of 100 cm/h, corresponding to 6 min residence time. In all studies the resins were regenerated and stored using 0.5 N NaOH and 0.1 N NaOH, respectively.

Confocal Microscopy

Finite Bath Experiments

Confocal microscopy experiments were performed to understand the capacity trends at the bead level. Monoclonal antibodies were labeled with Cy5 (GE Healthcare). To avoid light attenuation due to reabsorption or inner filtering (Ljunglöf, 2002; Ljunglöf and Hjorth, 1996; Ljunglöf and Thömmes, 1998; Van Oostvelt and Bauwens, 1990), the labeled protein was mixed with unlabeled protein in a ratio of 1:20. 20 mL protein solution (i.e., ~8 mg/mL in various buffers) was filled in a reaction vessel equipped with a hanging stirrer. The reaction vessel was connected to a Multitemp II water bath (GE Healthcare), and the temperature was set to 21°C. The adsorption experiment was started by adding a defined amount of gel slurry (i.e., settled gel diluted 1:2 with buffer) to the stirred protein solution. Samples were then taken from the reaction vessel at fixed times, and the adsorbent particles were analyzed by confocal microscopy within approximately 30 s. At the end of the finite bath experiment, the equilibrium capacity (Q_{eq}) was calculated indirectly from the decrease in protein concentration ($C_0 - C_{eq}$) according to Equation 2.

$$Q_{eq} = \frac{V_M(C_0 - C_{eq})}{V_S} \quad (2)$$

where V_M = volume of mobile phase, V_S = volume of solid phase, C_0 = initial protein concentration, and C_{eq} = protein concentration at equilibrium.

Individual adsorbent particles were analyzed by acquisition of two-dimensional confocal images perpendicular to the optical axis (i.e., xy-scan) (Ljunglöf, 2002; Ljunglöf and Hjorth, 1996; Ljunglöf and Thömmes, 1998). A 63 × 1.2 water immersion objective was used for all measurements. The laser provided excitation of Cy5 at 633 nm, and emitted fluorescent light was detected between 643 and 800 nm. To reduce background fluorescence and noise, the

images were generated by accumulating four scans per image. The image size was 512 × 512 pixels and the pixel size was 0.31 μm. The distribution of fluorescent molecules across the adsorbent particles was obtained by translating the confocal images into fluorescence intensity profiles (Ljunglöf, 2002; Ljunglöf and Hjorth, 1996; Ljunglöf and Thömmes, 1998). The overall fluorescence within the particles and the relative solid phase concentration (Q_{rel}) was calculated as previously described (Ljunglöf and Thömmes, 1998). By subsequently relating the relative fluorescence intensity obtained at different times to the value at equilibrium (Q_{rel}^{∞}), the degree of saturation versus time (F) could be calculated according to Equation 3 (Ljunglöf and Thömmes, 1998).

$$F = \frac{Q_{rel}}{Q_{rel}^{\infty}} \tag{3}$$

The solid phase concentration at different times during batch uptake was calculated from the equilibrium capacity, Q_{eq}, according to Equation 4:

$$Q_{solid} = F \times \frac{Q_{eq}}{(1-\varepsilon)} \tag{4}$$

Where ε = interparticle porosity.

Multi-Dye Analysis of Protein Adsorption

Multi-dye analysis was performed according to the method developed by Linden et al. (2002). The method is based on the consecutive incubation of adsorbent particles with the same protein but with different fluorophores. To ensure a continuity of the fluid phase conditions during batch adsorption studies, three finite bath incubations, with differently labeled but otherwise identical protein composition, are performed simultaneously. Mab1 was labeled with Cy3, Cy5 (GE Heathcare) and Alexa 488 (Molecular Probes), and mixed with unlabeled protein as described above. Three 2 mL tubes were filled with 1 mL of each protein solution. The initial protein concentration was equal in all batches (7 mg/mL). The uptake experiment was started by adding a defined volume of gel slurry (i.e., 25 μL settled gel diluted 1:2 with buffer). The tubes were incubated for a defined time in an end-over-end rotator. A sample (''Mab1-Cy3'') of 0.07 mL was taken from the Mab1-Cy3 tube, and was immediately analyzed by confocal microscopy. The Mab1-Cy3 and Mab1-Cy5 batches were centrifuged, whereupon the supernatant from the Cy3-tube was replaced with the Mab1-Cy5 supernatant. The two remaining batches (''Mab1-Cy3-Cy5'' and ''Mab1-Alexa'') were further incubated for a second period of time. A new sample was then removed from the ''Mab1-Cy3-Cy5 tube'' for confocal analysis, whereupon the Mab1-Cy5 supernatant was replaced with Mab1-Alexa. The final tube (''Mab1-Cy3-Cy5-Alexa'') was then incubated over night, after which a new sample was removed for confocal analysis. Multi-component confocal scanning was carried out in a sequential scan mode employing the following wavelength settings: Alexa 488 (excitation 488 nm, emission 505–530 nm), Cy3 (ex. 543 nm, em. 560–615 nm) and Cy5 (ex. 633 nm, em. 643–800 nm).

The experimental approach has earlier been evaluated (Linden et al., 2002). To ensure that covalent coupling of fluorescent dyes Cy3, Cy5, Alexa 488, and Oregon Green (Molecular Probes) does not influence equilibrium and kinetics, the isoelectric points of BSA and monoclonal IgG dye conjugates were determined. No significant deviations could be observed. Furthermore, the adsorption properties were verified by analyzing the retention of the various protein-dye conjugates in gradient elution from a cation exchanger (SP Sepharose Fast Flow). The maximum deviation between the retention time of labeled and unlabeled protein was 3%. Therefore, it was concluded that the adsorption of neither BSA nor IgG is significantly influenced by the coupling of fluorescent dyes (Linden et al., 2002). Control experiments have also been performed with sequential incubation using different combinations of labeled proteins (Cy3, Cy5, and Alexa 488). All combinations gave the same result. Thus, the different dyes did not have any major impact on the adsorption pattern (Linden, 2001; Ljunglöf, 2002).

Resin Characterization Study

The resin characterization was performed to study changes in pore accessibility of the resins with pH and conductivity. Pore accessibility was assessed by calculating distribution coefficients (Eq. 5) (Hagel, 1996, 1998; Hagel et al., 1996).

$$K_d = \frac{V_r - V_o}{V_t - V_o} \tag{5}$$

where K_d = distribution coefficient, V_r = peak retention volume, V_o = excluded or void volume, and V_t = included volume or total liquid volume of the column.

The distribution coefficient presents a measure of the pore accessibility. For example, a distribution coefficient of 0 implies that the solute is completely excluded or the pore is inaccessible. A distribution coefficient of 1 implies that the solute is completely included or the pore is fully accessible. The included and excluded volumes were obtained using the glucose and 2,000 kDa dextran retention times, respectively. Experiments were performed at pH 4, 6 and conductivities of 1, 5, and 50 mS/cm on SP Sepharose XL and SP Sepharose Fast Flow. The resin was equilibrated for 5 CV with the appropriate buffers (pH 4 or 6, and conductivities 1, 5, or 50 mS/cm). 1, 10, 40, 110, 500, 800, and 2,000 kDa dextran solutions (1 mg/mL) with glucose (1 mg/mL) and sodium azide (0.01%) were prepared as outlined in Proteins, Chemicals, and Resins section. The dextran solutions with glucose were then injected serially onto the column using a 500 μL sample loop (500 μg each of dextran and glucose). Equilibration buffer flow through the column was continued for 2 CV after each injection. Dextran and glucose retention times were obtained by measuring the refractive indices. The refractive indices were measured from the start of the dextran

DOI 10.1002/bit

injection to the end of the buffer flow for 2 CV. The distribution coefficient (K_d) was calculated according to Equation 5. Retention times of dextran and glucose were computed from the peaks of the refractive index traces stored on the ÄKTA system using the evaluation mode in the Unicorn™ 3.0 software.

RESULTS

Protein Dynamic Binding Capacity

Dynamic binding capacity trends were obtained as a function of pH and conductivity (Figs. 2, 3, and 4). The capacity trends obtained for both SP Sepharose XL and SP Sepharose Fast Flow displayed two domains. The first domain (positively sloped capacity trend) revealed unexpected behavior with capacity increasing with increasing conductivity. The capacity in this domain also increased with decreasing protein charge at the same conductivity. In the second domain (negatively sloped capacity trend) the capacity decreased with increasing conductivity as expected. The capacity also decreased with decreasing protein charge at equal conductivity.

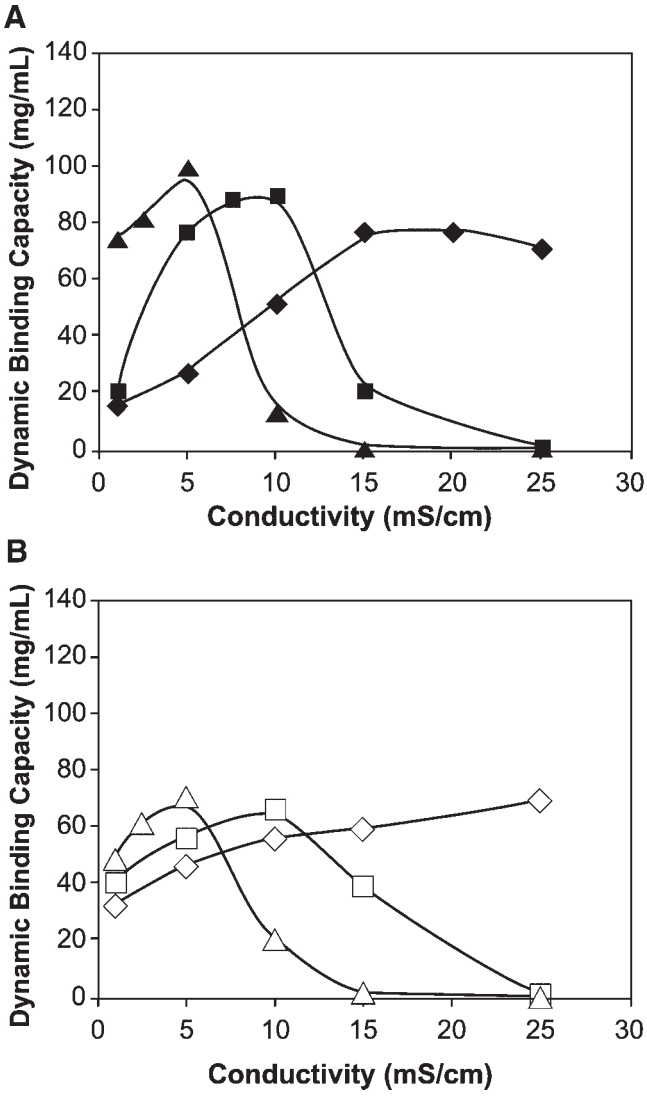

Figure 2. Dynamic binding capacity of Mab1 as a function of pH and conductivity (connecting lines used as visual aid) displaying unexpected positively sloped region and expected negatively sloped region on (**A**) SP XL, pH 4 (◆), 5 (■), and 6 (▲), (**B**) SP FF pH 4(◇), 5 (□), and 6 (△).

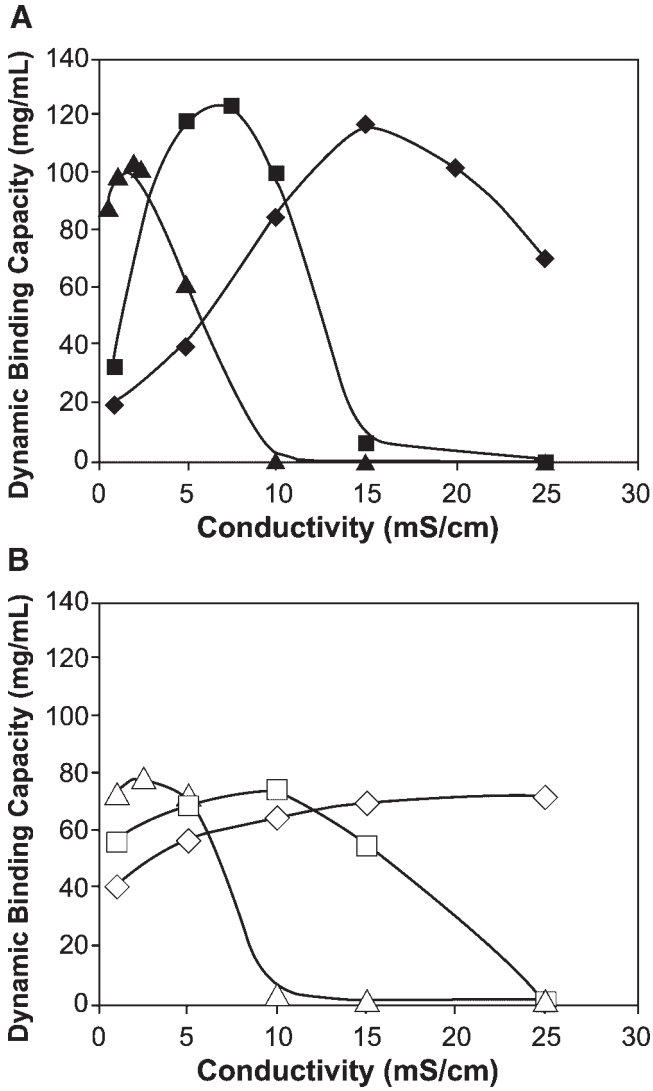

Figure 3. Dynamic binding capacity of Mab2 as a function of pH and conductivity (connecting lines used as visual aid) displaying unexpected positively sloped region and expected negatively sloped region on (**A**) SP XL, pH 4 (◆), 5 (■), and 6 (▲) (**B**) SP FF pH 4 (◇), 5 (□), and 6 (△).

The first domain may be explained by protein–protein charge-based exclusion as outlined below. The proteins initially entering the pore bind to the outer regions of the pore and due to charge repulsion (and in the case of very small pores steric hindrance) restrict subsequent protein from entering the pore. Note that conditions of low conductivity and high net protein charge support both strong protein–media attraction and protein–protein repulsion. However, the net charge of the protein decreases with increasing pH (Fig. 1). Furthermore, charge shielding by ions in solution

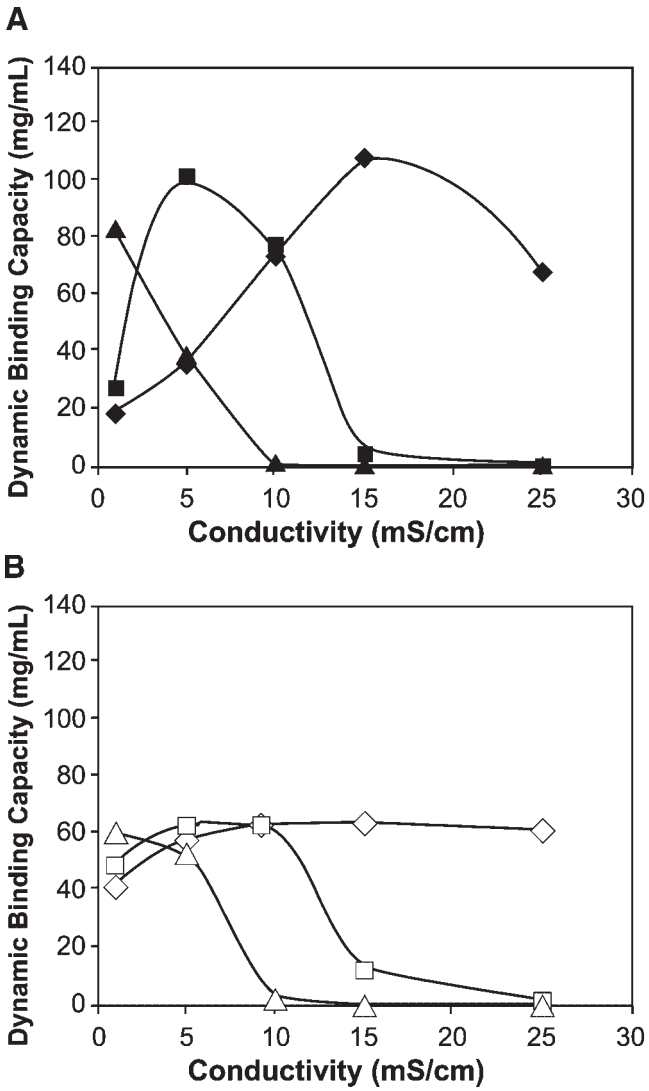

Figure 4. Dynamic binding capacity of Mab3 as a function of pH and conductivity (connecting lines used as visual aid) displaying unexpected positively sloped region and expected negatively sloped region on (**A**) SP XL, pH 4 (◆), 5 (■), and 6 (▲) (**B**) SP FF pH 4 (◇), 5 (□), and 6 (△).

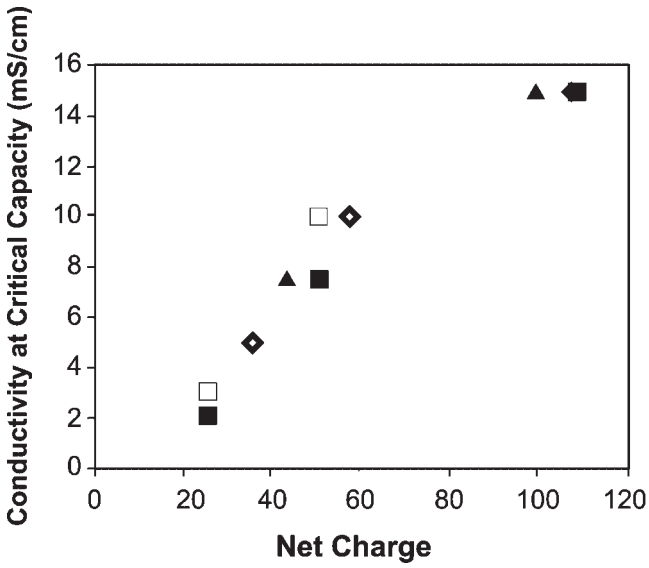

Figure 5. Conductivity at critical capacity as a function of net charge condenses into a single trend for: Mab1 on SP XL (◆) and SP FF (◇), Mab2 on SP XL (■) and SP FF (□) and Mab3 on SP XL (▲) and SP FF (△).

increases with increasing conductivity. Thus, increasing pH or conductivity decreases the above effects resulting in higher dynamic binding capacities. The behavior seen in the second domain is well understood. The electrostatic interactions between protein and pore decrease with increasing pH (reduced protein charge) or conductivity (charge shielding) resulting in decreased binding of the protein to the pore leading to decreasing capacities.

The dynamic binding capacity trends are in keeping with the above mechanistic explanations of the protein exclusion mechanism. The conductivity at which the optimum capacity occurs increases with decreasing pH, that is, increased protein net charge (Figs. 2–4). A combination of protein exclusion and equilibrium capacity appears to determine the overall dynamic binding capacity variation with pH and conductivity.

A "critical capacity" can be defined as the maximum dynamic binding capacity at the intersection of exclusion and equilibrium. It is seen that there is a direct relationship between protein net charge and the conductivity at which this critical capacity occurs (Fig. 5).

The dynamic binding capacity studies were performed as two or three replicates for each condition tested. Elution profiles for critical capacity conditions (pH 4, 15 mS/cm, pH 5, 10 mS/cm, pH 6, 5 mS/cm) for Mab1 on SP Sepharose XL are shown in Figure 6. Even under such high loading conditions chromatography worked well, good elution profiles were obtained and no apparent precipitation or viscosity issues were encountered. Even though the method was not optimized, yields of 90%, 81%, and 83% were obtained, respectively, for pH 4, 5, and 6.

Confocal Microscopy

Finite Bath Experiments

Confocal microscopy experiments were performed to understand the capacity trends at the bead level. As described in the Materials and Methods (Confocal Microscopy section), finite bath experiments were performed at varying pH and conductivity with SP Sepharose XL. By taking samples of the adsorbent particles at different times and measuring the fluorescence profile across the beads, the progression of protein uptake with experimental time could be visualized. An example is given in Figure 7, which shows a series of confocal images for the adsorption of Mab1 at pH 4. At low conductivity ($\leq$5 mS/cm), protein initially binds to the outer pore regions, after which the adsorption process proceeds very slowly. This provides direct visual evidence of protein–protein exclusion effects. By increasing the conductivity, the

DOI 10.1002/bit

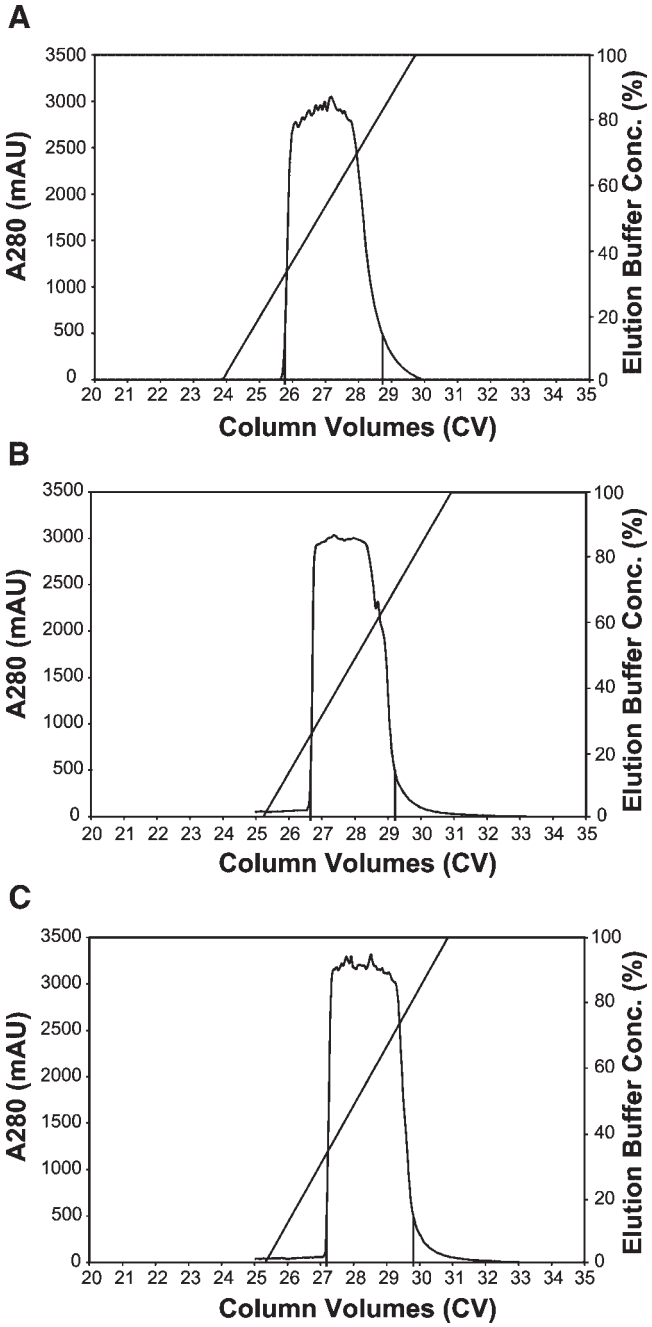

Figure 6. Chromatograms of critical capacity conditions for Mab1 on SP XL: (**A**) pH4, 15 mS/cm (**B**) pH5, 10 mS/cm (**C**) pH6, 5 mS/cm. It is to be noted that there is non-linearity in the absorbance measurements above 3,000 mAU. Elution pool concentrations for above conditions are (A) 24.1 mg/ml, (B) 28.4 mg/ml, and (C) 31.1 mg/ml respectively.

adsorption front moves faster into the particles and saturation is obtained much earlier. This is illustrated in Figure 8A, which shows the degree of saturation versus time (F). A comparison of mass uptake, Q_{solid} (g/L) over time (Fig. 8B) reveals that a higher uptake rate is obtained at increased conductivity. As expected, increased conductivity results in decreased equilibrium capacity (Q_{eq}) but faster mass transport into the particles results in greater capacity utilization, which leads to higher net dynamic capacity (Table III).

The finite bath experiments show that the highest uptake rate at pH 4 is obtained at 15 mS/cm. A summary of the confocal experiments performed with Mab1 is shown in Figure 9 and uptake curves for pH 5 and 6 in Figure 10. In conclusion, an increase in pH and/or conductivity results in higher velocity of the adsorption front, faster saturation of the adsorbent particles, higher uptake rate and greater dynamic capacity; even as the maximum equilibrium capacity decreases.

Multi-Color Analysis

Finite batch experiments were performed at three different experimental conditions. At low pH and conductivity (pH 5, 5 mS/cm) the protein molecules adsorb to the outer layer, and subsequent protein molecules are more or less excluded from the interior of the particle and continue to adsorb to free-binding sites in the outer layer (Fig. 11A). An increase in conductivity to 15 mS/cm results in a totally different adsorption pattern (Fig. 11B). The mass transport is much faster and the antibodies diffuse into the whole particle. Furthermore, a significant amount of the protein molecules that initially bound to the outer layer of the adsorbent continue to move towards the center of the particle. This allows newly incoming protein molecules to adsorb to free ligands at the rim. The final result is that all protein molecules are evenly distributed throughout the whole particle. This result is in accordance with Linden et al. (2002) who reported that changes in the mobile phase conditions (pH and ionic strength) lead to a switch in the protein uptake pattern for a monoclonal IgG2A. From a situation that appeared to be consistent with the physical picture of the shrinking core model, the protein uptake changed to a pattern where the protein molecules were transported further towards the particle core subsequent to binding to outer regions of the adsorbent.

Resin Characterization Study

An additional mechanism that could explain the first domain in the capacity trends is the pore accessibility of SP Sepharose XL increasing with conductivity due to increased flexibility of the dextran coating in the agarose matrix. The changes in pore accessibility of SP Sepharose XL and SP Sepharose Fast Flow were tested under varying conditions of pH and conductivity. As described in Resin Characterization Study section, 500 µL spikes of 1, 10, 40, 110, 500, 800, 2,000 kDa dextran solutions under the same conditions of pH, conductivity were injected serially into the column. The retention time of dextrans in the column was obtained and distribution coefficients were calculated. Distribution coefficients for the dextrans were recorded as a function of viscosity radii (R_η) for each pH and conductivity tested. For clarity, Table IV gives the viscosity radii for a distribution coefficient $K_d = 0.1$ as a function of pH and conductivity. As stated earlier in Resin Characterization Study Section, the distribution coefficient presents a measure of the pore

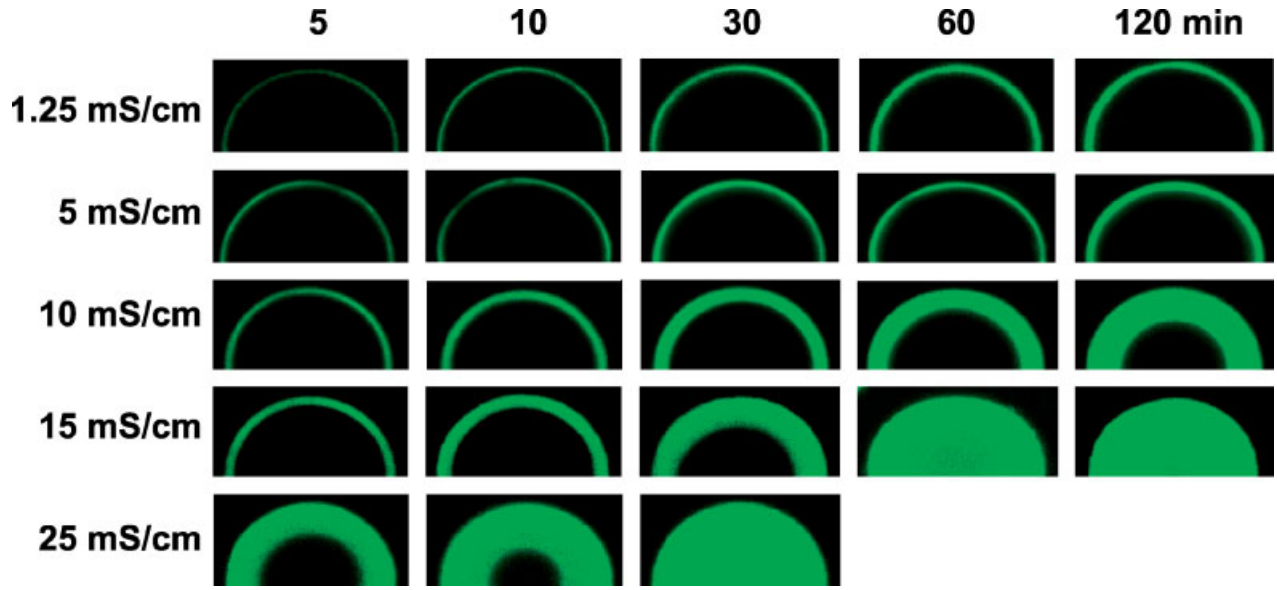

Figure 7. Confocal microscopy images: Mab1 uptake to SP XL during finite bath adsorption at pH 4, 1.25, 5, 10, 15, and 25 mS/cm. Images recorded at 5, 10, 30, 60, and 120 min.

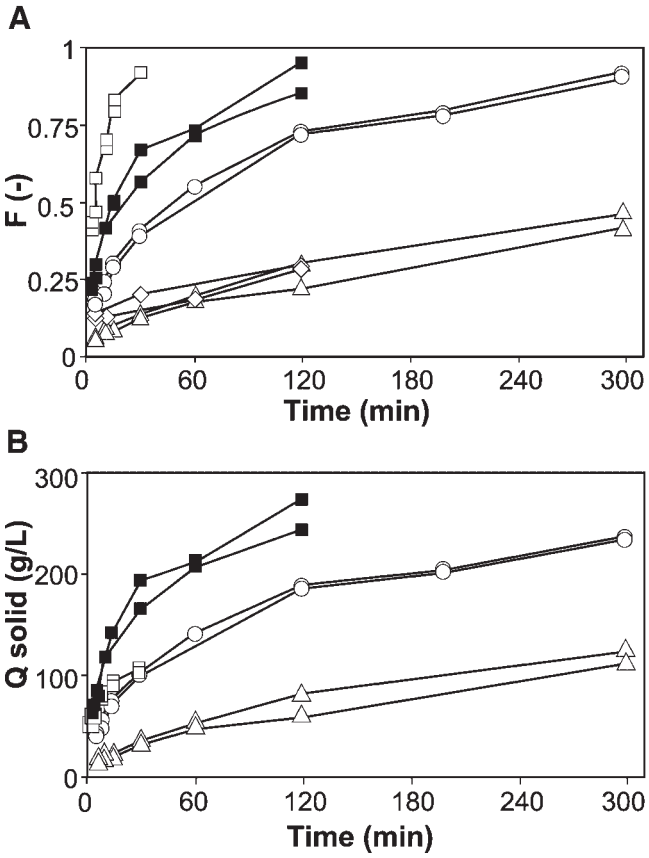

Figure 8. **A:** Fractional approach to equilibrium from finite bath adsorption of Mab1 to SP XL at pH 4, 1.25 mS/cm (△), 5 mS/cm (◇), 10 mS/cm (○), 15 mS/cm (■), and 25 mS/cm (□). **B:** Mass uptake curve from finite bath adsorption of Mab1 to SP XL at pH 4, 1.25 mS/cm (△), 10 mS/cm (○), 15 mS/cm (■), and 25 mS/cm (□).

accessibility (or partition) of uncharged dextran into the pores. It is seen (Table IV) that the pore accessibility (or K_d) increases with conductivity for SP Sepharose XL but does not change with conductivity for SP Sepharose Fast Flow. Pore accessibility is not altered with pH for either SP Sepharose XL or SP Sepharose Fast Flow.

DISCUSSION

Antibody dynamic binding capacity trends were investigated as a function of pH and conductivity on SP Sepharose XL and SP Sepharose Fast Flow. Media that are similar in porosity pore size distribution, SP type charge groups, and charge density (μmoles/mL media) and differ primarily in the Sepharose XL media pores containing a charged dextran polymer layer. The dynamic binding capacity and batch uptake studies displayed two domains. The first domain (positively sloped capacity trends) revealed capacity increasing with increasing conductivity. The capacity in this domain also increased with decreasing protein charge at the same conductivity. The second domain (negatively sloped capacity

Table III. Binding capacity and capacity utilization for Mab1 to SP Sepharose XL at varying pH and conductivity.

pH	Conductivity (mS/cm)	Q_B, 10% (g/L)	Q_{eq} (g/L)	Q_B/Q_{eq} (%)
4	1.26	15	232	6
4	10	50	175	29
4	25	75	78	96
5	1.3	25	289	9
5	10	90	109	83
5	15	25	28	89
6	1.2	75	154	49
6	5	100	104	96

DOI 10.1002/bit

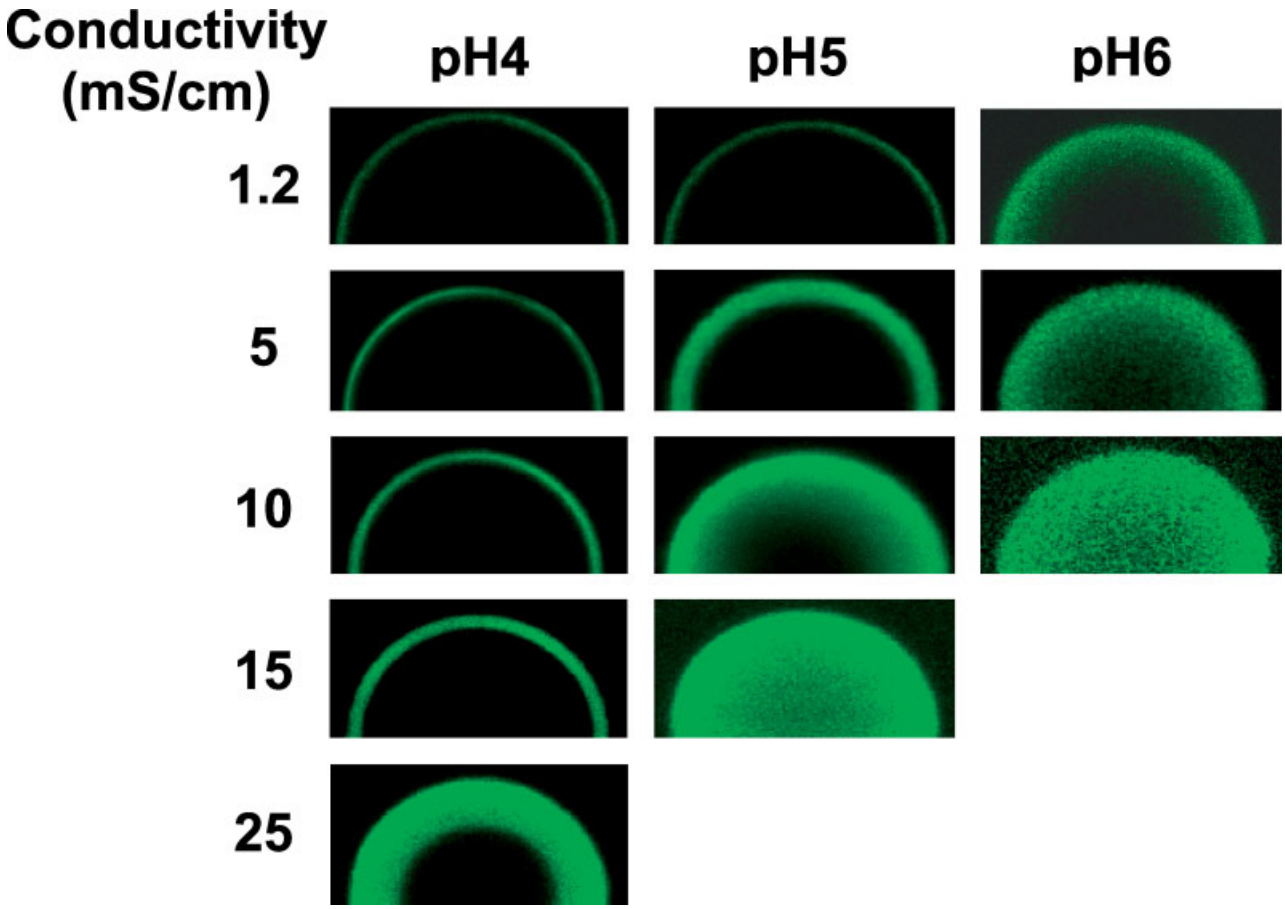

Figure 9. Confocal microscopy images recorded after 5 min: Mab1 uptake to SP XL during finite bath adsorption, pH 4, 5, 6, Conductivity: 1.25, 5, 10, 15, and 25 mS/cm.

trends) exhibited capacity decreasing with increasing conductivity. The capacity also decreased with decreasing protein charge at equal conductivity.

The region of negative slope is well characterized, but the region of positive slope is unexpected and cannot be explained by classic mechanisms of IEX. This region of positive slope (first domain) can be explained by a protein exclusion mechanism, which predicts capacities increasing with increasing conductivity and decreasing protein charge. Increasing pH (decreasing protein charge) and conductivity (increasing charge shielding) causes a decrease in the charge repulsion effects that appear to reduce protein transport and binding resulting in increased dynamic capacity. The results from over 300 chromatographic experiments (Figs. 2, 3, and 4) are consistent with this explanation.

More direct evidence of protein exclusion at low pH and conductivity was demonstrated by confocal microscopy. As seen from the confocal microscopy data at pH 4 and 1 mS/cm, the Mab1 binds to the outer layer of the bead (Fig. 7). Reduced protein exclusion (increased pore accessibility) and decreasing equilibrium capacity occur with increasing conductivity. This results in the optima seen in the capacity curves as well as the various influences of pH and conductivity. In addition, multi-color analysis (Fig. 11B) revealed that an increase in conductivity, results in increased mobility of protein molecules that initially bind to the outer layer of the adsorbent particles. This allows newly incoming protein molecules to adsorb to free ligands at the rim. The mass transport into the particles becomes much faster and the whole particle volume is utilized for protein adsorption, resulting in increased dynamic binding capacity.

The above-noted exclusion phenomena plus related chromatographic and microscopic results were seen with both SP Sepharose FF and SP Sepharose XL media. The major difference in these media types is that SP Sepharose XL contains charged dextran polymers. NMR studies have shown that random movement of these polymers increases with conductivity (Herbert Baumann, GE Healthcare, private communication). Not surprisingly, transport of neutral dextran polymer standards through such pores appears to increase with conductivity in SP Sepharose XL media though not in SP Sepharose Fast Flow media (Table IV). An increase in the flexibility of such ion exchange group tethering polymers might favor both increased protein transport (through the dextran layer) and more favorable protein–ligand interactions resulting in greater equilibrium capacity. Not surprisingly SP Sepharose XL media typically accounted for the highest dynamic capacities seen under various conditions. However, the extent of the capacity differences recorded suggest that while such effects of the dextran

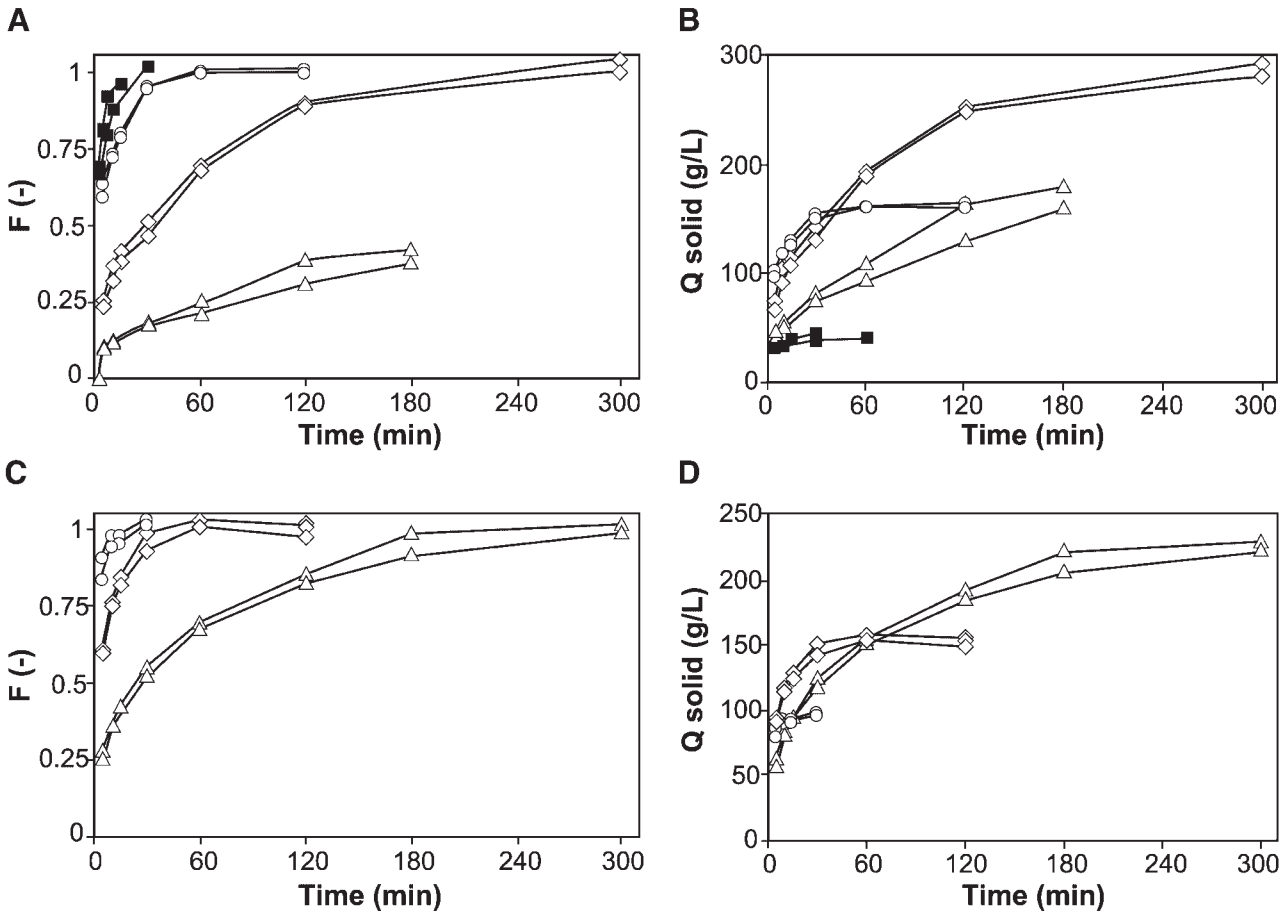

Figure 10. **A:** Fractional approach to equilibrium from finite bath adsorption of Mab1 to SP XL at pH 5: 1.25 mS/cm (△), 5 mS/cm (◇), 10 mS/cm (○), and 15 mS/cm (■). **B:** Mass uptake curve from finite bath adsorption of Mab1 to SP XL at pH 5, 1.25mS/cm (△), 5 mS/cm (◇), 10 mS/cm (○), and 15 mS/cm (■). **C:** Fractional approach to equilibrium from finite bath adsorption of Mab1 to SP XL at pH 6, 1.25 mS/cm (△), 5 mS/cm (◇), and 10 mS/cm (○). **D:** Mass uptake curve from finite bath adsorption of Mab1 to SP XL at pH 6, 1.25 mS/cm (△), 5 mS/cm (◇), and 10 mS/cm (○).

polymers can be significant, they appear to (a) be secondary in degree to exclusion effects, and (b) exert less influence on the degree of exclusion effects than do other matrix properties or operating variables.

Other investigators have provided indirect evidence of this mechanism in ion exchange displacement chromatography (Malinova et al., 2004). This study was limited to a class of polyelectrolytes used as displacer molecules with fixed charges. It focuses on the effect of contour length, hydrophobicity of the substituent group and concentration of the polyelectrolytes at two ionic strengths on stationary phase adsorbent capacity. Inferences on the occurrence of the exclusion mechanism were restricted to comparisons of pore dimensions to the calculated geometric and electrostatic dimensions of the polyelectrolytes.

In the present work dynamic binding capacity, batch uptake and confocal microscopy, studies all suggest that protein exclusion mechanisms may function in IEX, and significantly influence dynamic protein binding capacities. Annual production requirements of antibodies for high dose chronic therapies are in the order of a metric ton for each product. Recent advances in expression levels will enable production of 100 kg batches that will significantly contribute to increased plant capacity and reduced cost of goods. Higher capacity ion exchange resins and related processes will be required to meet these increased batch sizes. The application of the exclusion mechanism in optimization of ion exchange, process and resin development will help meet these increasing demands.

In addition to the practical significance of the present work, it is therefore of interest to explore to what extent it provides general insight into ion exchange process interactions and optimization. Figure 5 provides a graph of protein net charge versus the conductivity at which critical capacity occurs. As such it represents results from several hundred chromatograms, which normally might be undertaken (to greater or lesser degree) when optimizing a process. The graph basically reduces to a straight line such that only a few measurements undertaken at high protein net charge and conductivity would be required to construct a rough plot and gain insight to which operating "regions" of conductivity might provide optimal dynamic capacity for similar sized proteins of similar net charge (pH) or vice versa. Note that the graph suggests where to expect optimal dynamic capacity for any set of conditions, but not which set of conditions will supply the greatest capacity.

DOI 10.1002/bit

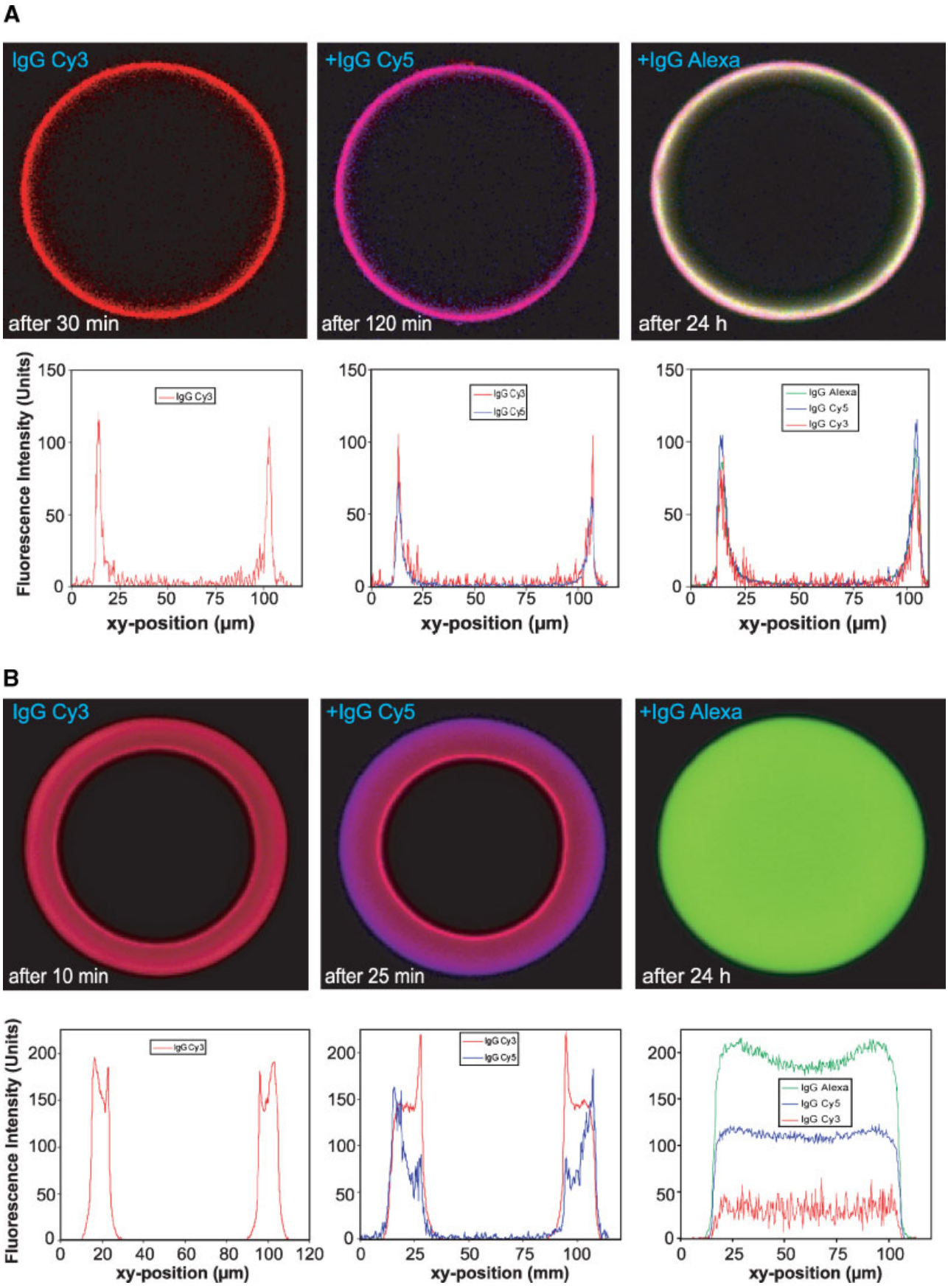

Figure 11. **A:** Confocal microscopy images (three dye experiments) demonstrating protein exclusion at low conductivities and pH: Mab1 on SP XL, pH 4, 5 mS/cm. **B:** Confocal microscopy images (three dye experiments): Mab1 on SP XL, pH 4, 15 mS/cm.

Table IV. Pore accessibility data from resin characterization study.

		R_h for $K_d = 0.1$	
pH	Conductivity (mS/cm)	SP Sepharose FF	SP Sepharose XL
4	1	15	4
4	5	15	4.5
4	50	15	7
4	1	15.2	4
6	1	15.2	4

It is encouraging that the general interactions summarized by Figure 5 appear to vary little for media as different in construction as SP Sepharose Fast Flow and SP Sepharose XL. So is the fact that the relationship noted holds for three different Mabs; as long as their charge nature was related to net surface charge. Ishihara et al. (2005) recently reported that a fairly large family of Mabs showed SP Sepharose Fast Flow peak elution behavior which varied in relation to surface net positive charge of their V_H region. As such their results support belief that the present work will apply to a wider range of proteins.

The present study illustrates how one design factor (inclusion of dextran layers in ion exchange media) can positively affect the above-noted phenomena and lead to improved dynamic capacity under conditions of higher conductivity. Studies are underway to further elucidate other matrix-related effects, as well as protein-related effects—via both laboratory experimentation and theoretical modeling.

The linearity expressed in Figure 5 may actually represent more general ion exchange phenomena related to media and protein surface potentials and their influence over the balance of attraction between media and free protein, and repulsion between adsorbed and free protein. Such a hypothesis may provide a path to reconciling present findings with a wider range of media and proteins as well as the work of earlier scientists (e.g., Dziennik et al., 2003; Pujar and Zydney, 1998) and the obvious complexity of protein transport and binding in charged hydrogels (Carlsson et al., 2001; Lewus and Carta, 2001; Liapis et al., 2001).

As evidenced by the present work, and those noted above, advances in analytical methods (such as laser scanning confocal microscopy) and various modeling approaches reveal ever more complex transport and adsorption phenomena in IEX. The significance, under some conditions, of phenomena such as intra-pore electrophoretic transport is becoming more fully appreciated (e.g., Liapis and Grimes, 2005) as are the molecular level interactions responsible for such phenomena. Recent publications by Zhang et al. (2004b, 2005a,b) provide example of the use of such simulations in ion exchange, and their application to complex systems similar to those studied here. Faced with such complexity, scientists working with bioprocess optimization must have readily assimilated and applicable simplifications to use in daily operation.

The value of the present work and recognition of the practical significance of exclusion effects is not just in showing that common assumptions about ion exchange operating parameters such as conductivity or pH may be wrong but in providing fundamental insights into IEX and a basis to improve related media and processes.

References

Brooks CA, Cramer S. 1992. Steric mass-action ion exchange: Displacement profiles and induced salt gradients. AIChE J 38(12):1969.

Carlsson F, Linse P, Malmsten M. 2001. Monte Carlo simulations of polyelectrolyte-protein complexation. J Phys Chem B 105:9040–9049.

Chang C, Lenhoff AM. 1998. Comparison of protein adsorption isotherms and uptake rates in preparative cation-exchange materials. J Chromatogr A 827:281.

Dziennik SR, Belcher EB, Barker GA, DeBergalis MJ, Fernandez SE, Lenhoff AM. 2003. Nondiffusive mechanisms enhance protein uptake rates in ion exchange particles. Proc Nat Acad Sci USA 100:420.

Gagnon P. 1996. Purification tools for monoclonal antibodies. ISBN 0-9653515-9-9, Validated Biosystems, Tucson, AZ, 1996.

Gallant SR. 2004. Modeling ion exchange adsorption of proteins in a spherical particle. J Chromatogr A 1028(2):189.

Hagel L. 1988. Pore size distribution. In: Dubin PL, editor. Aqueous Size-Exclusion Chromatography. Amsterdam: Elsevier. p 119.

Hagel L. 1996. Characteristics of modern media in aqueous size exclusion chromatography. In: Potschka M, Dubin PL, editors. Strategies in Size Exclusion Chromatography (ACS Symposium Series 635). Washington, DC: American Chemical Society. p 225.

Hagel L. 1998. Gel filtration. In: Janson JC, Ryden L, editors. Protein Purification–Principles, high resolution methods, and applications. New York: Wiley-VHC. p 79.

Hagel L, Östberg M, Andersson T. 1996. Apparent pore size distributions of chromatography media. J Chromatogr A 743:33.

Harinarayan C, Mueller J, Ljunglöf A, Fahrner R, van Reis R. 2002. Development of novel ion exchange process conditions in antibody purification. Presentation at Antibody Production and Downstream Processing, IBC conference, San Diego, USA, November 18, 2002.

Hubbuch J, Linden T, Knieps E, Thömmes J, Kula MR. 2002. Dynamics of protein uptake within the adsorbent particle during packed bed chromatography. Biotechnol Bioeng 80(4):359.

Hubbuch J, Linden T, Knieps E, Thommes J, Kula MR. 2003. Mechanism and kinetics of transport in chromatography media studied by confocal laser scanning microscopy. Part II. Impact on chromatographic separations. J Chromatogr A 1021:105.

Hunter AK, Carta G. 2000. Protein adsorption on novel acrylamido-based polymeric ion exchangers. J Chromatogr A 897(1–2):81.

Ishihara T, Kadoya T, Yoshida H, Tamada T, Yamamoto S. 2005. Rationale for predicting human monoclonal antibodies retention in protein A affinity chromatography and cation exchange chromatography. Structure-based chromatography design for monoclonal antibodies. J Chromatogr A 1093:126–138.

Janson JC, Ryden L. 1998. Protein Purification–Principles, high resolution methods, and applications. New York: Wiley-VHC.

Kasche V, De Boer M, Lazo C, Gad M. 2003. Direct observation of intraparticle equilibrium and the rate-limiting step in adsorption of proteins in chromatographic adsorbents with confocal laser canning microscopy. J Chromatogr B 790:115.

Laca A, Garcia LA, Argueso F, Dias M. 1999. Protein diffusion in alginate beads monitored by confocal microscopy. The application of wavelets for data reconstruction and analysis. J Industr Microbiol Biotechnol 23: 155.

Lewus RK, Carta G. 2001. Protein transport in constrained anionic hydrogels: Diffusion and boundary-layer mass transfer. Ind Eng Chem Res 40:1548.

DOI 10.1002/bit

Liapis AI, Grimes BA. 2005. The coupling of the electrostatic potential with the transport and adsorption mechanism in ion exchange chromatography systems: Theory and experiments. J Sep Sci 28:1909.

Liapis AI, Grimes BA, Lacki K, Neretnieks I. 2001. Modeling and analysis of the dynamic behavior of mechanisms that result in the development of inner radial humps in the concentration of a single adsorbate in the adsorbed phase of porous adsorbent particles observed in confocal scanning laser microscopy experiments: Diffusional mass transfer and adsorption in the presence of an electrical double layer. J Chromatogr A 291:135.

Linden T. 2001. Doctoral thesis: ''Untersuchungen zum inneren Transport bei der Proteinadsorption an poröse Medien mittels konfokaler Laser-Raster-Mikroskopie''. Heinrich-Heine-Universität Duesseldorf, Germany.

Linden T, Ljunglöf A, Kula MR, Thömmes J. 1999. Visualizing two-component protein diffusion in porous adsorbents by confocal scanning laser microscopy. Biotechnol Bioeng 65(6):622.

Linden T, Ljunglöf A, Hagel L, Kula MR, Thömmes J. 2002. Visualizing patterns of protein uptake to porous media using confocal scanning laser microscopy. Separation Sci Technol 70:1.

Ljunglöf A. 2002. Doctoral thesis: ''Direct observation of biomolecule adsorption and spatial distribution of functional groups in chromatographic adsorbent particles''. Uppsala University, Sweden. www.uu.se/avhandlingar.

Ljunglöf A, Hjorth R. 1996. Confocal microscopy as a tool for studying protein adsorption to chromatographic matrices. J Chromatogr A 743: 75.

Ljunglöf A, Thömmes J. 1998. Visualizing intraparticle protein transport in porous adsorbents by confocal microscopy. J Chromatogr A 813:387.

Malinova V, Freitag R, Wandrey C. 2004. Adsorption of charged macromolecules on oppositely charged porous column materials. J Chromatogr A 1036:25.

Nash DC, Chase H. 1998. Comparison of diffusion and diffusion-convection matrices for use in ion-exchange separations of proteins. J Chromatogr A 807:185.

Potschka M. 1988. Size exclusion chromatography of polyelectrolytes: Experimental evidence for a general mechanism. J Chromatogr A 441: 239.

Pujar NS, Zydney AL. 1994. Electrostatic and electrokinetic interactions during protein transport through narrow pore membranes. Ind Eng Chem Res 33:2473.

Pujar NS, Zydney AL. 1998. Electrostatic effects on protein partitioning in size-exclusion chromatography and membrane ultrafiltration. J Chromatogr A 796:229.

Saksena S, Zydney AL. 1994. Effect of solution pH and ionic strength on the separation of Albumin from Immunoglobulins (IgG) by selective filtration. Biotech Bioeng 43:960.

Smith FG, Deen WM. 1980. Electrostatic double-layer interactions for spherical colloids in cylindrical pores. J Colloid Interface Sci 78:444.

Van Oostvelt P, Bauwens S. 1990. Quantitative fluorescence in confocal microscopy. The effect of the detection pinhole on the re-absorption and inner filtering phenomena. J Microscopy 158:121.

van Reis R. 2005. Downstream Keynote. Charge exclusion phenomena in separation media. Abstracts of Papers, Best of Biochemical Technology Division of ACS, July 18, 2005.

van Reis R, Brake JM, Charkoudian J, Burns DB, Zydney AL. 1999. High-performance tangential flow filtration using charged membranes. J Membrane Sci 159:133.

Zhang X, Grimes BA, Wang J-C, Lacki KM, Liapis AI. 2004a. Analysis and parametric sensitivity of the behavior of overshoots in the concentration of a charged adsorbate in the adsorbed phase of charged adsorbent particles: practical implications for separation of charged solutes. J Colloid Interface Sci 273:22.

Zhang X, Wang J-C, Lacki KM, Liapis AI. 2004b. Molecular Dynamics Simulation studies of the transport and adsorption of a charged macromolecule onto a charged adsorbent solid surface immersed in an electrolytic solution. J Colloid Interface Sci 277:483.

Zhang X, Wang J-C, Lacki KM, Liapis AI. 2005a. Molecular Dynamics Simulation studies of the conformation and lateral mobility of a charged adsorbate biomolecule: Implications for estimating the critical value of the radius of pore in porous media. J Colloid Interface Sci 290:373.

Zhang X, Wang J-C, Lacki KM, Liapis AI. 2005b. Construction of molecular dynamics modeling and simulations of the porous structures formed by dextran polymer chains attached on the surface of the pores of a base matrix: Characterization of porous structures. J Phys Chem 109: 21028.